*remote sensing*

MDPI

*Article*

# Advancing the Solar Radiation Pressure Model for BeiDou-3 IGSO Satellites

**Fengyu Xia [1,2], Shirong Ye [1,*], Dezhong Chen [1], Longjiang Tang [3,4], Chen Wang [5], Maorong Ge [2,4] and Frank Neitzel [2]**

[1] GNSS Research Center, Wuhan University, 129 Luoyu Road, Wuhan 430079, China; fengyuxia@whu.edu.cn (F.X.); chendz@whu.edu.cn (D.C.)
[2] Institute of Geodesy and Geoinformation Science, Technische Universität Berlin, Straße des 17. Juni 135, 10623 Berlin, Germany; maorong.ge@gfz-potsdam.de (M.G.); frank.neitzel@tu-berlin.de (F.N.)
[3] School of Geomatics, Liaoning Technical University, Fuxin 123000, China; longjt@gfz-potsdam.de
[4] German Research Centre for Geosciences (GFZ), 14473 Potsdam, Germany
[5] College of Geology Engineering and Geomatics, Chang'an University, Xi'an 710054, China; chen.wang@chd.edu.cn
* Correspondence: srye@whu.edu.cn

**Abstract:** In the absence of detailed surface information, empirical solar radiation pressure (SRP) models, such as the five-parameter Empirical CODE Orbit Model (ECOM1) and its extended version-ECOM2, are widely used for modeling SRP forces acting on GNSS satellites. This study shows that the orbits of BeiDou-3 Inclined Geosynchronous Orbit satellites (IGSOs) determined with the ECOM1 model suffer from systematic once-per-revolution radial orbit errors, which can be partly reduced by the ECOM2 model. To eliminate such orbit errors, the BeiDou-3 IGSO optical coefficients are solved by using an adjustable box-wing (ABW) model and then introduced into an a priori box-wing SRP model to enhance the ECOM1 model (ECOM1 + BW). In the ABW solution, in addition to satellite body and solar panels, the contributions of the communication payloads installed on BeiDou-3 IGSO $\pm X$ panels on the SRP are also considered, which markedly improves the stability of the optical coefficient estimates. The efficiency of the developed a priori box-wing model is demonstrated through eliminated once-per-revolution radial orbit errors and decreased day boundary discontinuities. However, the orbit solutions still show significant degradations during eclipse seasons. The results of the first yaw-attitude analysis for eclipsing BeiDou-3 IGSOs show that their yaw behaviors are the same as those of BeiDou-3 CAST (China Academy of Space Technology) MEOs (Medium Earth Orbit satellites), and have been well considered in the study. This rules out the possibility that attitude errors are the potential reason for the orbit deterioration. By introducing a once-per-revolution sine term in the Sun direction ($D_s$ term) and keeping $D_s$ active during the Earth's shadow transitions to the ECOM1 + BW model, the orbit performance inside the eclipse seasons is significantly improved and can be comparable to that outside the eclipse seasons.

**Keywords:** solar radiation pressure; BeiDou-3 IGSOs; box-wing model; eclipse seasons; yaw-attitude

check for updates

**Citation:** Xia, F.; Ye, S.; Chen, D.; Tang, L.; Wang, C.; Ge, M.; Neitzel, F. Advancing the Solar Radiation Pressure Model for BeiDou-3 IGSO Satellites. *Remote Sens.* **2022**, *14*, 1460. https://doi.org/10.3390/rs14061460

Academic Editor: Roberto Peron

Received: 4 February 2022
Accepted: 15 March 2022
Published: 18 March 2022

**Publisher's Note:** MDPI stays neutral with regard to jurisdictional claims in published maps and institutional affiliations.

**Copyright:** © 2022 by the authors. Licensee MDPI, Basel, Switzerland. This article is an open access article distributed under the terms and conditions of the Creative Commons Attribution (CC BY) license (https://creativecommons.org/licenses/by/4.0/).

## 1. Introduction

The third-generation BeiDou Navigation Satellite System (BeiDou-3) announced its operational services for the global region on 31 July 2020. The BeiDou-3 constellation consists of 3 satellites in Geostationary Orbit (GEO), 3 in Inclined Geosynchronous Orbit (IGSO) and 24 in Medium Earth Orbit (MEO) [1]. Compared with the regional BeiDou satellite navigation system (BeiDou-2), BeiDou-3 satellites are equipped with inter-satellite links (ISLs) payloads and adds three new services signals, namely B1C at 1575.42 MHz, B2a at 1176.45 MHz and B2b at 1207.14 MHz [2,3]. The updated rubidium atomic frequency standards (RAFSs) and passive hydrogen masers (PHMs) have been used by BeiDou-3 satellites. The stability of these new onboard atomic clocks has been improved by a factor of

10 compared with the RAFSs adopted onboard the BeiDou-2 satellites, and can be compared to the RAFSs employed onboard the GPS III satellites, as well as the PHMs used onboard the Galileo satellites [4].

The high-accuracy orbit and clock products are key requirements for the most demanding applications of the BeiDou satellites [5,6]. Solar radiation pressure (SRP) is the largest non-gravitational perturbation for high-altitude satellites and constitutes a major challenge for navigation satellite systems that require cm-level orbit knowledge. The perturbing accelerations aroused by SRP for a satellite depends on its attitude, mass and dimensions as well as the optical properties of each surface facing the Sun [7]. Without precise surface information, the five-parameter Empirical CODE Orbit Model (ECOM) [8], developed at the Center for Orbit Determination in Europe (CODE), is widely applied for GNSS precise orbit determination (POD). However, for satellites of newly emerging systems, the model must be adapted and optimized as systematic once-per-revolution radial orbit errors were found. For example, the orbits of European Galileo and Japanese QZSS satellites with rectangular shapes based on the five-parameter ECOM model suffer from radial orbit errors with an orbital periodicity [9,10]. Montenbruck et al. [9] identified that the stretched shape of navigation satellites introduces additional accelerations that cannot be considered by the ECOM model as the cause for these systematic radial orbit errors. Such errors in the Galileo and QZSS orbits have been proved to be reduced by using the extended ECOM model (ECOM2) [11,12] or almost eliminated by adopting an a priori high-accuracy SRP model with the ECOM [9,10].

A similar orbit error has been found while using the legacy five-parameter ECOM model for BeiDou-3 MEOs with a notably stretched body [13–15]. This can be confirmed by the BeiDou-3 MEO clock estimates and Satellite Laser Ranging (SLR) residuals. Based on the adjustable box-wing model (ABW) with clear physical interpretation for SRP [16], the a priori SRP models for BeiDou-3 MEOs have been established by Yan et al. [14] and Wang et al. [13], which could effectively reduce the systematic radial orbit errors.

According to the BeiDou-3 metadata released by [17], BeiDou-3 IGSOs exhibit a notably rectangular shape. Hence, similar to BeiDou-3 MEOs, Galileo and QZSS, the BeiDou-3 IGSO orbits determined with the five-parameter ECOM model may also suffer from systematic radial orbit errors. More information from China Satellite Navigation Office (CSNO) demonstrates that BeiDou-3 IGSOs carry a regular hexagon and two circular communication payloads on the $\pm X$ surfaces, as shown in Figure 1. There is a challenge to model BDS-3 IGSO SRP perturbations, as the contribution of communication payloads should be considered [18,19]. Moreover, the GNSS orbits always show a lower performance during eclipse seasons than non-eclipse seasons. It is usually caused by the inaccurate attitude modeling [20] and unaccounted non-conservative forces, such as spacecraft's thermal effects during eclipse seasons [21–23]. At present, there is no systematic investigation on the POD performance of eclipsing BeiDou-3 IGSOs.

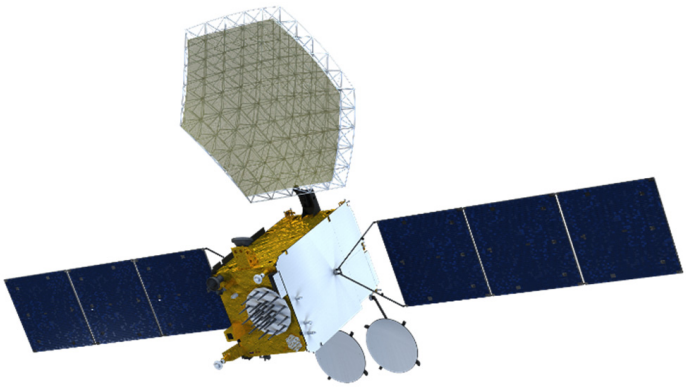

**Figure 1.** BeiDou-3 IGSOs unfolding on-orbit (http://www.csno-tarc.cn/en/system/introduction (accessed on 15 November 2021)).

Overall, currently, there are no published studies on the SRP modeling of BeiDou-3 IGSOs and the POD performance of BeiDou-3 IGSOs during eclipse seasons. The purpose of this study is to carry out the SRP modeling for BeiDou-3 IGSOs and to investigate and improve their orbit performance during eclipse seasons.

First, the ECOM, ECOM2 and box-wing (BW) models are introduced. The data collection and POD processing strategies are then presented as the study is to a large extent based on numerical investigation. An a priori BW model is established by estimating the optical properties of BeiDou-3 IGSOs. The performance of the five-parameter ECOM model with and without this a priori BW model, as well as the seven-parameter ECOM2 model, is evaluated. An effective strategy for improving eclipsing BeiDou-3 IGSOs orbit performance is recommended. Finally, the key conclusions are summarized.

## 2. Materials and Methods

### *2.1. ECOM-Type Models*

To improve GPS orbit accuracy, the ECOM model was developed in the 1990s [8]. The ECOM models the SRP force in a Sun-oriented $DYB$ frame with axes $D$ pointing from the satellite to the Sun, $Y$ along the solar panel axis, and $B$ completing a right-handed system. The modelled force in each direction is described by a constant and optional periodic terms depending on the satellite's argument of latitude $u$, which is expressed as follows [8]:

$$\begin{aligned} a_D &= D_0 + D_c \cos u + D_s \sin u \\ a_Y &= Y_0 + Y_c \cos u + Y_s \sin u \\ a_B &= B_0 + B_c \cos u + B_s \sin u \end{aligned} \tag{1}$$

In general, only five parameters $D_0$, $Y_0$, $B_0$, $B_c$, $B_s$ are estimated for the proper modeling of SRP forces acting on GPS satellites, which is called the five-parameter ECOM model or ECOM1 model. It is worth mentioning that some studies show that the $D_s$ term should be considered during eclipse seasons and kept also active during Earth's shadow transitions because it helps to improve the orbit quality during eclipse seasons [22,23]. In this study, the ECOM1 model with the $D_s$ term active also in Earth's shadows is named the ECOM1D model.

However, as mentioned earlier, the ECOM1 model has been found to cause systematic once-per-revolution radial orbit errors for navigation satellites with a notably stretched body, such as Galileo and BeiDou-3 MEOs [9,13]. In order to cope with this systematic effect, the extended ECOM model (ECOM2) was developed [11]:

$$\begin{aligned} a_D &= D_0 + \sum_{i=1}^{n_D} \{D_{2i,c} \cos(2i\Delta u) + D_{2i,s} \sin(2i\Delta u)\} \\ a_Y &= Y_0 \\ a_B &= B_0 + \sum_{i=1}^{n_B} \{B_{2i-1,c} \cos((2i-1)\Delta u) + B_{2i-1,s} \sin((2i-1)\Delta u)\} \end{aligned} \tag{2}$$

where $\Delta u$ is the difference between the satellite's argument of the latitude and the Sun's argument of the latitude in the orbital plane, and the upper limit values $n_D$ and $n_B$ are defined by users. At the beginning of 2015, the nine-parameter ECOM2 model $(n_D = 2, n_B = 1)$ was recommended by CODE. Since 28 June 2015, the estimated parameter number of the ECOM2 model in CODE products was reduced from 9 to 7 by excluding 4-times-per-revolution parameters as they deteriorated the GLONASS orbit solutions [24]. Following the CODE data processing strategy, the seven-parameter ECOM2 model $(n_D = 1, n_B = 1)$ is used in this study.

### *2.2. Box-Wing Model*

The ECOM1 model can also be applied if a proper box-wing model is involved to consider the systematic impact caused by the stretched satellite shape. The structure of a GNSS satellite can be simplified to a cuboid body with six faces (box) plus solar

panels (wings). Total SRP acceleration can be theoretically obtained by summing the SRP acceleration for each illuminated satellite surface and solar panel. This modeling method, commonly referred to as the box-wing model, was originally established for Topex/Poseidon POD [25]. According to Milani et al. [26], the acceleration produced by the physical interaction between the solar radiation and a flat surface of the satellites can be formulated by:

$$a = -\frac{A}{M}\frac{S_0}{c}\cos\theta\left[(\alpha+\delta)\vec{e}_D + 2(\frac{\delta}{3}+\rho\cos\theta)\vec{e}_N\right] \tag{3}$$

where $S_0$ is the total solar irradiance at the 1 AU, and $M$ is the satellite's mass. The parameter $c$ is the velocity of light and $A$ is the illuminated surface area. The terms $\vec{e}_D$ and $\vec{e}_N$ indicate the satellite-Sun unit vector, and the normal vector of the illuminated surface, respectively. The term $\theta$ is the angle between $\vec{e}_D$ and $\vec{e}_N$, and the parameters $\alpha$, $\delta$ and $\rho$ (with $\alpha+\delta+\rho=1$, Milani et al. [26]) are the absorption, diffuse and specular reflection coefficients of illuminated surface, respectively.

Under the assumption of mostly balanced thermal re-mission from the front and back-side of the solar panels, the SRP acceleration $a_{sp}$ on the satellite solar panels can be described by using Equation (3) [16]. For the nominal attitude [27], the satellite solar panels are perpendicular to the Sun direction with $\cos\theta_{sp}=1$ and $\vec{e}_{N,sp}=\vec{e}_D$. Equation (3) can be reformulated as [16]:

$$a_{sp} = -\frac{A}{M}\frac{S_0}{c}\left[(1+\rho+\frac{2}{3}\delta)\vec{e}_D\right] \tag{4}$$

The satellite bus is covered by multilayer insulation for thermal protection. According to Lambert's law, the accelerations $a_{i,th}$ aroused by the immediate thermal re-radiation from the satellite bus surfaces can be obtained by [7]:

$$a_{i,th} = -\frac{A}{M}\frac{S_0}{c}\cos\theta\frac{2}{3}\alpha\vec{e}_N \tag{5}$$

where subscript $i$ represents the illuminated satellite body surface. According to the IGS convention [27], for satellite bodies in nominal attitude, only their $+X$, $+Z$, $-Z$ surfaces are illuminated by the Sun.

By adding the instantaneous thermal re-radiation accelerations $a_{i,th}$ to Equation (3), the accelerations $a_b$ acting on satellite bus are expressed as [16]:

$$a_b = -\frac{A}{M}\frac{S_0}{c}\cos\theta\left[(\alpha+\delta)(\vec{e}_D+\frac{2}{3}\vec{e}_N)+2\rho\cos\theta\vec{e}_N\right] \tag{6}$$

Currently, only the absorption coefficient $\alpha$ for BeiDou-3 IGSO surfaces is disclosed by CSNO [17], which hinders the formation of a proper BW model. Therefore, in the study, the adjustable box-wing model developed by [16] is used to solve the optical coefficients for BeiDou-3 IGSOs with real tracking measurements. For the satellites in nominal attitude, there are nine estimated parameters in the ABW model, i.e., the absorption plus diffuse reflection $(\alpha+\delta)$ as well as the specular reflection $(\rho)$ for each illuminated satellite surface $(+X,+Z,-Z)$, the scale parameter for solar panels $1+\rho+\frac{2}{3}\delta$, and two non-optical parameters $Y$ bias $(Y_0)$ and solar panel rotation lag angle $(SB)$.

From Equations (4) and (6), the partial derivatives of the acceleration w.r.t the optical properties of the satellite bus and panel surfaces can be obtained as [16]:

$$\frac{\partial a_b}{\partial(\alpha_i+\delta_i)} = -\frac{A_i}{M}\frac{S_0}{c}\cos\theta_i(\vec{e}_D+\frac{2}{3}\vec{e}_{N,i}) \tag{7}$$

$$\frac{\partial a_b}{\partial\rho_i} = -\frac{A_i}{M}\frac{S_0}{c}2\cos^2\theta_i\cdot\vec{e}_{N,i} \tag{8}$$

$$\frac{\partial a_{sp}}{\partial(1+\rho+\frac{2}{3}\delta)_{sp}} = -\frac{A_{sp}}{M}\frac{S_0}{c}\vec{e}_D \tag{9}$$

Two non-optical parameters, i.e., $SB$ and $Y_0$, are considered in the ABW model to compensate for the potential misalignments of the solar panels around the $Y$-axis and constant accelerations along the $Y$-axis, respectively. The $Y_0$ parameter of the ABW model is the same as that of the ECOM-type models. The partial derivatives of the acceleration w.r.t parameter $SB$ can be obtained as [16]:

$$\frac{\partial a_{sp}}{\partial SB} = -\frac{A_{sp}}{M}\frac{S_0}{c}2(\frac{\delta_{sp}}{3}+\rho_{sp})sign(\dot{\varepsilon})\vec{e}_B \tag{10}$$

where $\vec{e}_B$ is the unit vector of the $B$-axis of Sun-oriented $DYB$ frame [8], and $\varepsilon$ is Sun–spacecraft–Earth angle, which can be expressed as:

$$\cos\varepsilon = \cos\beta\cos U \tag{11}$$

where $\beta$ is the sun elevation angle above the satellite orbital plane, and $U$ is a geocentric orbit angle between the satellite and the midnight point in the orbital plane.

### *2.3. BeiDou-3 IGSOs' Structure*

Based on the above description, the knowledge of satellite structure information is the prerequisite to conducting the ABW solution. From the BeiDou-3 metadata released by CSNO [17], the box-shaped body of BeiDou-3 IGSOs has, essentially, a rectangular cross-section of 2.098 × 2.358 m, and a length of 3.602 m. Moreover, BeiDou-3 IGSOs carry a regular hexagon and two circular communication payloads on the $\pm X$ surfaces, as shown in Figure 1. These payloads will not only increase the illuminated area of $\pm Z$ surfaces but also may shadow the $+X$ surfaces. Unfortunately, the installation information (angle, location and distance relative to the spacecraft body) and dimensions for these payloads are not disclosed.

In this study, the following assumptions were made for the ABW solution. The radius of the two circular payloads is 0.5 m, and the side length of the regular hexagon payload is the same as that of the $Y$ side of the spacecraft's body. These payloads are mounted vertically on $\pm X$ surfaces, and the resulting SRP perturbations are treated in the same way as for the $\pm Z$ surfaces by simply increasing the area. Considering that the specific distance and installation locations for these payloads, relative to the spacecraft body, are not available, the potential shading effects are neglected. The coarse reference values for BeiDou-3 IGSO geometrical dimensions and optical properties are given in Table 1. Since the diffuse and specular reflection coefficients are not yet released, their initial values are assumed to be 0 and $1-\alpha$, respectively. Optical parameters of satellite surfaces are adjusted following the same procedures as Rodriguez-Solano et al. [16].

**Table 1.** Reference values of optical absorption $\alpha$, reflectivity $\delta$, and diffusion $\rho$ as well as geometrical dimensions of satellite bus and solar panels (SPs) for BeiDou-3 IGSOs. Values in brackets were the areas of $\pm Z$ panels without considering communication payloads. The unit of Area is $m^2$.

| Panel | Area | $\alpha$ | $\delta$ | $\rho$ |
|---|---|---|---|---|
| $+X$ | 8.496 | 0.350 | 0 | 0.650 |
| $+Z$ | 20.871 (4.956) | 0.870 | 0 | 0.130 |
| $-Z$ | 20.871 (4.956) | 0.870 | 0 | 0.130 |
| SPs | 17.700 | 0.920 | 0 | 0.080 |

## 3. Results

In this study, 15 months of GNSS data from 1 January 2020 to 31 March 2021, collected by 21 iGMAS (International GNSS Monitoring and Assessment Service) stations [28] and 34 Multi-GNSS Experiment (MGEX) stations [29], were selected to determine precise orbits

and clocks, and their distribution is illustrated in Figure 2. The data processing was divided into the following two steps. In the first step, a static GPS/Galileo precise point positioning (PPP) solution is conducted for each station using the GFZ (GeoForschungsZentrum) MGEX products including precise orbits, 30-s clocks and Earth orientation parameters. In the second step, the station coordinates, zenith troposphere delays and receiver clock parameters obtained in the first step are kept fixed to determine BeiDou-3 IGSO orbits and clocks, ambiguities and inter-system bias (ISB) as well as SRP parameters. In data processing, the ionospheric-free combination of BeiDou-3 B1I/B3I, GPS L1/L2 and Galileo E1/E5a dual-frequency observations are used. Due to the sparse BeiDou-3 IGSO tracking network, data of a 2-day arc is computed to strengthen the solution. The first day of 2-day-arc solutions is extracted as the final daily solution in this study. General data processing settings are listed in Table 2.

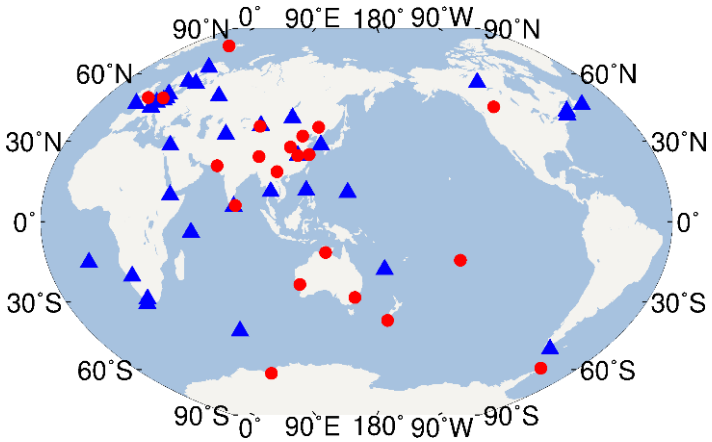


**Figure 2.** Distribution of GNSS tracking stations used for the BeiDou-3 IGSO POD. Red circles are iGMAS stations, and blue triangles represent MGEX stations.

**Table 2.** Summary of precise orbit determination strategies.

| Item | Description |
|---|---|
| Software | PANDA [30] |
| Orbits | Initial positions and velocities |
| Clocks | Estimated as white noise |
| Elevation cutoff | 5° |
| Sampling | 5 min |
| Weight | Elevation-dependent weighting: $\sin(E)$ |
| Initial standard deviations | 10 mm and 1 m for ionospheric-free combination carrier phase and pseudo-range, respectively |
| Gravitational forces | Earth, Sun/Moon/Planets (DE405), solid earth, ocean and pole tides |
| Relativistic effects | IERS conventions 2010 [31] |
| Attitude model | GPS/Galileo [32], BeiDou-3 IGSOs [33] |
| Antenna thrust | igs_metadata_2081.snx |
| Ambiguity | Fixed for BeiDou-3 IGSOs [34] |
| Receiver ISB | Estimated as constants for each receiver |
| Antenna phase center model | Satellite antenna PCOs and PCVs of GPS L1/L2, Galileo E1/E5a and BeiDou B1I/B3I from igs14_2097.atx. For BeiDou and Galileo receiver antenna, the corrections for GPS L1/L2 are used for the BeiDou B1I/B3I and Galileo E1/E5a as their calibrations are unavailable in the igs14_2097.atx |

There are various SRP models involved in data processing. The ABW model is employed to estimate the surface optical coefficients, which are either not yet available or are inaccurate, but definitely needed for establishing a proper BW model for BeiDou-

3 IGSOs. The ECOM1 and ECOM2 models are used to demonstrate their insufficiency for BeiDou-3 IGSOs, and the impact of the BW model is shown by the comparison of the ECOM1/ECOM2 and ECOM1 with the developed BW model. The ECOM1D + BW model suggested in the study shows a significant improvement in orbit quality during eclipse seasons.

### *3.1. BeiDou-3 IGSO Optical Properties Estimates*

In this section, the adjusted optical parameters of BeiDou-3 IGSOs are discussed. Satellite C39 is selected as an example for BeiDou-3 IGSOs. Figure 3 illustrates the estimated optical coefficients for satellite C39 without and with considering communication payloads as a function of $\beta$ -angle. To make the presentation of Figure 3 more concise, the absorption plus diffuse reflection $(\alpha + \delta)$, as well as the specular reflection $(\rho)$ parameters, are denoted by the words "AD" and "R", respectively. It can be clearly seen that the stability of optical parameters is improved significantly when the contribution of communication payloads on $\pm X$ surfaces to SRP perturbations is taken into account. This is closer to the fact that the satellite optical properties do not change from day to day. In the study, the adjusted optical coefficients for satellite bus with communication payloads are involved in the a priori box-wing model (Equation (3)) to enhance the ECOM1 model. The optical coefficient estimates for solar panels are not used because the contribution of solar panels can be well covered through the $D_0$ term of empirical SRP models. Table 3 gives the adjusted box-wing optical coefficients for the BeiDou-3 IGSOs' satellite bus, which are acquired by averaging the daily corresponding estimates for all BeiDou-3 IGSOs during the experiment period.

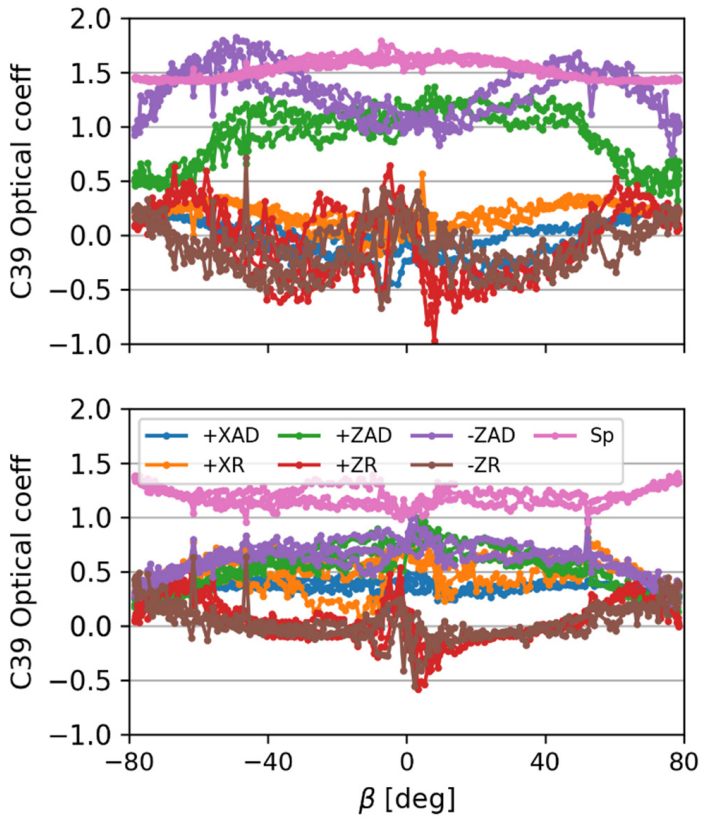


**Figure 3.** Estimated optical coefficient of the box-wing model for satellite C39 without (**top**) and with (**bottom**) considering communication payloads. The words "AD" and "R" represent the absorption plus diffuse reflection $(\alpha + \delta)$ as well as the specular reflection $(\rho)$ for illuminated surfaces, respectively.

**Table 3.** Estimated optical absorption plus reflectivity $(\alpha + \delta)$ and diffusion $(\rho)$ as well as corresponding standard deviations for all BeiDou-3 IGSOs' satellite bus. The unit of Area is $m^2$.

| Panel | Area | α+δ | ρ |
|---|---|---|---|
| $+X$ | 8.496 | $0.366 \pm 0.048$ | $0.531 \pm 0.165$ |
| $+Z$ | 20.871 | $0.589 \pm 0.169$ | $0.001 \pm 0.172$ |
| $-Z$ | 20.871 | $0.662 \pm 0.123$ | $0.018 \pm 0.143$ |

### *3.2. Performance of SRP Models for BeiDou-3 IGSO Satellites*

As mentioned earlier, due to BeiDou-3 IGSO satellites with a cuboid shape, the orbits determined with the ECOM1 model may have systematic radial orbit errors. Therefore, the performance of ECOM1, ECOM2 and ECOM1 + BW models for BeiDou-3 IGSO orbit determination is analyzed. Although all BeiDou-3 IGSOs are equipped with laser retroreflectors for Satellite Laser Ranging that allows for external accuracy assessment of orbit radial component, none of BeiDou-3 IGSOs have been tracked by the International Laser Ranging Service so far. Other than SLR, the clock estimates of high-stable satellite clocks can also be used as a quality indicator for radial orbit modeling issues because radial orbit errors are mapped to the estimated satellite clocks [9,12,15,23]. Due to the PHM clocks equipped on BeiDou-3 IGSOs, the residuals of the daily estimated clocks after a second-order polynomial fitting are used as a measure of radial orbit accuracy. Of course, the orbit boundary discontinuity (DBD) [35] is also a very important index for assessing orbit quality and will be discussed in detail.

#### 3.2.1. Orbit Assessment Based on Estimated Clocks

Figure 4 illustrates the fitting residual RMS of daily clock estimates for satellite C39 from the POD solutions with the ECOM1, ECOM2 and ECOM1 + BW models. For each solution, the clock fitting residual RMS of three BeiDou-3 IGSOs, C38, C39 and C40, exhibit similar patterns. From Figure 4, the RMS time series based on the ECOM1 model show pronounced $\beta$ -dependent variations with peak-to-peak amplitude of about 13.0 cm. The stable and small RMS values only occur for very short time periods when the $|\beta|$ is greater than 60°. Once the ECOM2 model is used, this $\beta$ -dependent effect is weakened, but still significant. The solution with the ECOM1 + BW model gives the best results, and the systematic effects are almost eliminated. Table 4 lists the mean of daily clock residual RMS of satellites C38, C39 and C40 for the ECOM1, ECOM2 and ECOM1 + BW solutions. The mean of daily clock residual RMS for the ECOM1 + BW solution decreases by 3.2 cm (47.1%) and 1.4 cm (28.0%) relative to the ECOM1 and ECOM2 solutions on average, respectively.

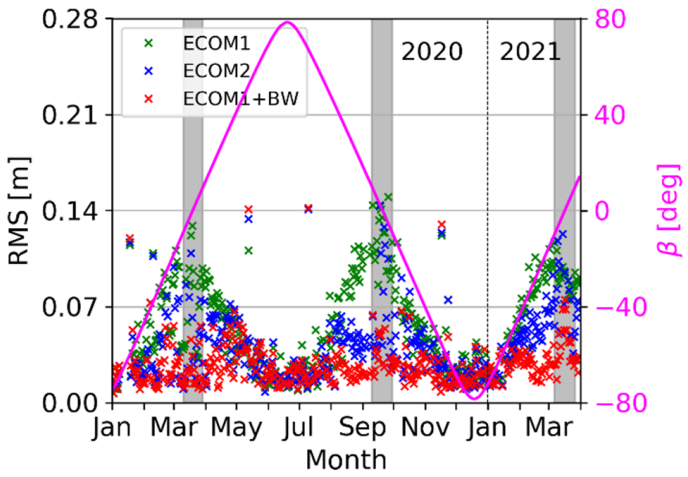


**Figure 4.** Daily RMS of clock fitting residuals for satellite C39 based on the ECOM1 (green), ECOM2 (blue) and ECOM1 + BW (red) models. The areas shaded in gray indicate eclipse seasons.

**Table 4.** Mean of daily fitting residual RMS of BeiDou-3 IGSO clocks for the solutions with the ECOM1, ECOM2 and ECOM1 + BW models in cm.

| Satellite | ECOM1 | ECOM2 | ECOM1 + BW |
|---|---|---|---|
| C38 | 7.8 | 6.1 | 4.1 |
| C39 | 5.7 | 4.1 | 2.8 |
| C40 | 6.9 | 4.8 | 3.3 |

A significant part of the systematic $\beta$ -dependent pattern in the clock fitting residual RMS for the ECOM1 solution is induced by radial orbit modeling defects, which can be confirmed by the clock residual time series on DOY 172–173, 2020 ($\beta \approx 78.4°$) and DOY 254–255, 2020 ($\beta \approx 9.5°$) presented in Figure 5. During DOY 254–255 of the year 2020, there is a once-per-revolution signal with an amplitude of roughly 20 cm in the clock fitting residuals, resulting in a large clock residual RMS. The major reason is that the ECOM1 model cannot fully consider the effect of the rapidly varying cross-section exposed to the Sun on SRP during periods with small $\beta$ -angles, which introduces systematic once-per-revolution radial orbit errors [9]. This systematic error can be reduced by using the ECOM2 model or almost eliminated when using the developed a priori box-wing model, as shown in Figure 5. For the periods with a large $\beta$ -angle on DOY 172–173 of the year 2020, the illuminated cross-section of the satellite body does not change much. The ECOM1 model can work as efficiently as the ECOM2 and ECOM1 + BW models in this scenario (Figure 5, top). The SRP modeling defects of the ECOM1 model leads to this systematic $\beta$ -dependent pattern in the clock fitting residual RMS.

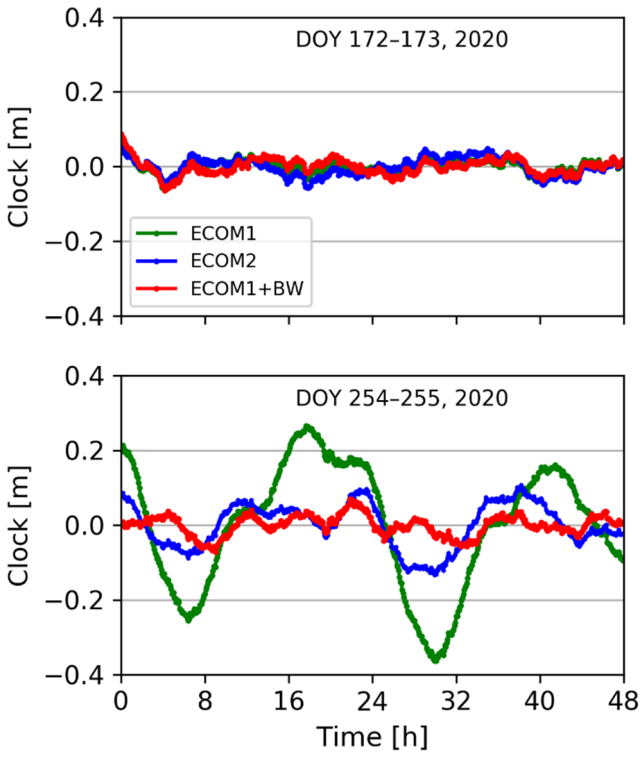


**Figure 5.** Satellite C39 clock fitting residuals for the ECOM1 (green), ECOM2 (blue) and ECOM1 + BW (red) solutions on DOY 172–173, 2020 (**top**), $\beta \approx 78.4°$) and DOY 254–255, 2020 (**bottom**), $\beta \approx 9.5°$).

Although the clock residual RMS of BeiDou-3 IGSOs can be effectively reduced by using the a priori box-wing model, they are still large in the eclipse seasons. Table 5 gives the mean of daily clock residual RMS of BeiDou-3 IGSOs for the ECOM1 + BW solution inside and outside eclipse seasons. After entering eclipse seasons, the clock residual RMS increases by an average of 0.6 cm (20.9%). In particular, the clock estimates of eclipsing

satellite C39 deteriorated most severely, with an increase of 0.7 cm (26.9%) in the fitting residual RMS.

**Table 5.** Mean of daily fitting residual RMS of BeiDou-3 IGSO clocks for the solutions with the ECOM1 + BW and ECOM1D + BW models insides and outsides eclipse seasons in cm. "NE" and "E" denotes the non-eclipse and eclipse seasons, respectively.

| SRP Model | C38 | | C39 | | C40 | |
|---|---|---|---|---|---|---|
| | NE | E | NE | E | NE | E |
| ECOM1 + BW | 3.9 | 4.2 | 2.6 | 3.3 | 3.1 | 3.8 |
| ECOM1D + BW | - | 4.0 | - | 2.3 | - | 3.5 |

In order to illustrate the clock behaviors of eclipsing BeiDou-3 IGSOs in detail, Figure 6 gives the time series of clock fitting residual RMS for satellite C39 based on the ECOM1 + BW model during one eclipse season (days 58–90 of the year 2021). With the decrease of $|\beta|$, the clock residual RMS is significantly elevated. This clearly indicates the presence of orbit modeling deficiencies during eclipse seasons.

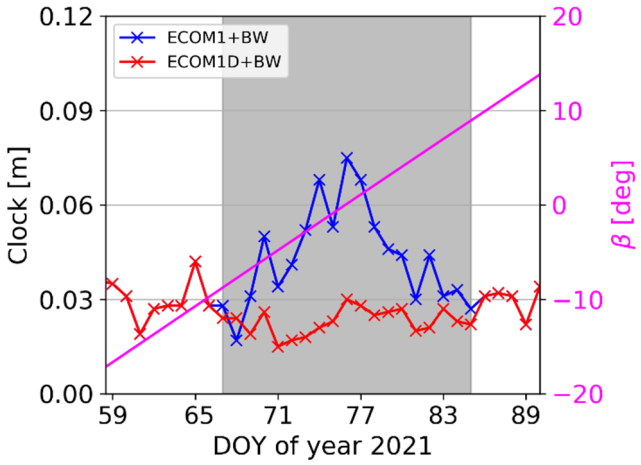


**Figure 6.** Daily RMS of clock fitting residuals for satellite C39 based on the ECOM1 + BW (blue) and ECOM1D + BW (red) models over DOY 58–90, 2021. The area shaded in gray indicates eclipse seasons.

As mentioned earlier, there are generally two reasons for the orbit solution degradation of eclipsing satellites. One is the inaccurate attitude modeling [20], and the other is the unexplained non-conservative forces, such as thermal effects from spacecraft's body [21–23]. Based on reverse kinematic PPP (RTPPP), which is proposed by Dilssner et al. [36] to monitor and model the yaw behaviors of eclipsing satellites, we perform the first analysis for the yaw-attitude maneuvers of eclipsing BeiDou-3 IGSOs. RKPPP estimates, nominal values [27] and predicted values using the BeiDou continuous yaw-attitude (CYS) model [13,33] for the yaw angle of satellite C39 in the vicinity of the midnight and noon points are illustrated in Figures 7 and 8. The BeiDou CYS model, developed by [13,33] for the new BeiDou-2 I06 and later proved to be also applicable to the BeiDou-3 CAST (China Academy of Space Technology, Beijing, China) MEOs, is expressed as follows:

$$\Psi(U_s) = a\tan 2(-\tan\beta, \sin U_s) \tag{12}$$

$$\Psi(U) = 90^\circ \cdot SIGN(1, \Psi(U_s)) + [\Psi(U_s) - 90^\circ \cdot SIGN(1, \Psi(U_s))] \cdot \cos(\frac{2\pi}{t_{\max}} \cdot \frac{U - U_s}{\dot{U}}) \tag{13}$$

where $U_s$ is the orbit angle at the start of the yaw maneuver. The best value of $U_s$ is $-6^\circ$ or $174^\circ$. The term $t_{\max}$ is a constant, which represents the duration of the yaw maneuver.

The values are 3090 s and 5740 s for MEO and IGSO satellites, respectively. $\Psi(U)$ is the modelled yaw angle at the orbit angle $U$.

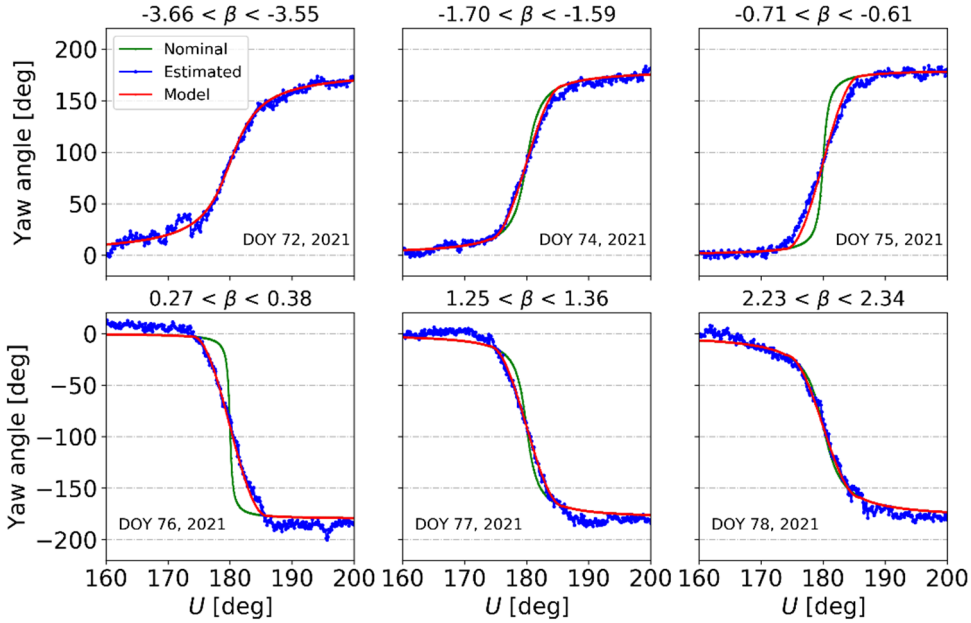


**Figure 7.** Nominal (green), estimated (blue) and modeled (red) yaw angles of IGSO C39 crossing the noon point at different $\beta$ -angles.

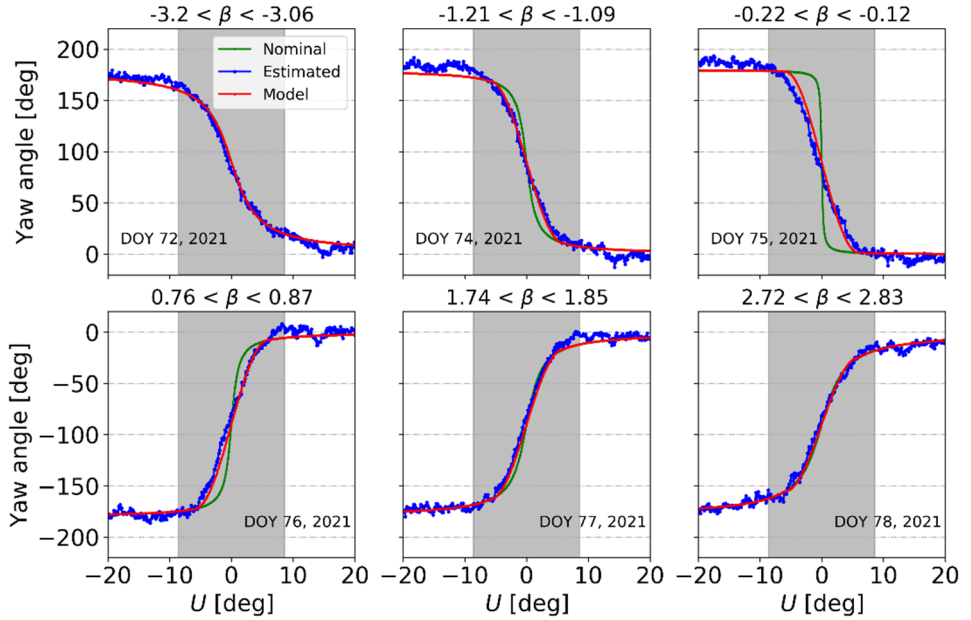


**Figure 8.** Nominal (green), estimated (blue) and modeled (red) yaw angles of IGSO C39 passing the Earth's shadow (gray area) under different $\beta$ -angles.

From Figures 7 and 8, the yaw maneuvers of BeiDou-3 IGSOs occur when the $\beta$ -angle is in the range of $[-3°, 3°]$ and the $U$ angle is in the range of approximately $[-6°, 6°]$ or $[174°, 186°]$. The yaw behaviors of eclipsing BeiDou-3 IGSOs can be well reproduced by the BeiDou continuous yaw-attitude model used in this study [13,33]. This rules out the first assumption that attitude errors may be the reason for the orbit deterioration and suggests the presence of unmodeled non-conservative orbit perturbations during eclipse seasons.

The signal presented in the BeiDou-3 IGSO clock fitting residuals (Figure 6) can be also observed in the Galileo FOC (Full Operational Capability) satellites during eclipse seasons [37]. Previous studies confirmed that the deterioration of Galileo FOC clocks estimates was attributed to the unaccounted thermal radiations from the spacecraft body, and this modeling deficiency can be compensated by the estimation of the $D_s$ parameter during eclipse seasons and also keeping $D_s$ active during Earth's shadow transitions [22,23,37].

We found that adding the $D_s$ term in the ECOM1 + BW model and keeping it active in Earth's shadows., i.e., the ECOM1D + BW model, is very effective for eclipsing BeiDou-3 IGSOs. The mean of daily clock residual RMS of eclipsing BeiDou-3 IGSOs for the ECOM1D + BW solution is given in Table 5. Compared with the ECOM1 + BW solution, the clock residual RMS of eclipsing BeiDou-3 IGSOs decreases by 0.5 cm (13.3%) on average. The elevated clock residual RMS is well reduced, and the RMS statistics inside and outside the eclipse season are on the same level (Figure 6). To further highlight that the clock estimates benefit from the consideration of the $D_s$ term, the clock residuals of satellite C39 on DOY 74–75, 2021 ($\beta \approx -1.8°$) for the ECOM1 + BW and ECOM1D + BW solutions are shown in Figure 9. It can be seen that the stability of clock estimates based on the ECOM1 + BW model does not conform to the characteristics of PHM clocks on BeiDou-3 IGSOs. When switching the ECOM1 + BW model to the ECOM1D + BW model, the clock residuals become very stable. The above results clearly indicate that the orbit modeling defects of eclipsing BeiDou-3 IGSOs can be covered by the introduction of the $D_s$ term also active in Earth's shadows.

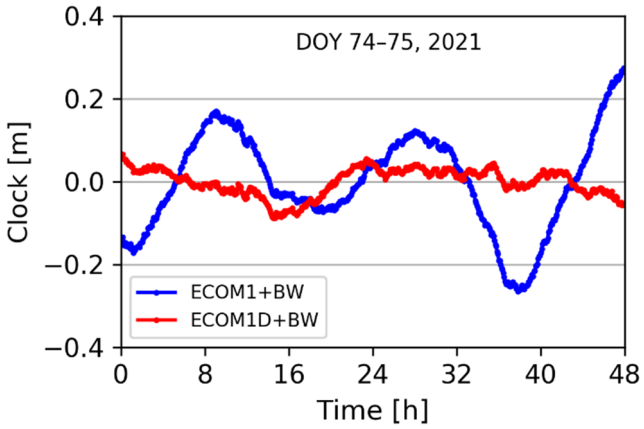


**Figure 9.** Satellite C39 clock fitting residuals for the ECOM1 + BW (blue) and ECOM1D + BW (red) solutions on DOY 74–75, 2021($\beta \approx -1.8°$).

3.2.2. Orbit Assessment Based on Orbit Boundary Discontinuities

The orbit DBD in the radial, along- and cross-track, and as well as three-dimension (3D) directions are defined as [35]:

$$(\Delta R, \Delta A, \Delta C)^T = M \cdot (X_{i+1} - X_i, Y_{i+1} - Y_i, Z_{i+1} - Z_i)^T \quad (14)$$

$$T_{3D} = \sqrt{(\Delta R)^2 + (\Delta A)^2 + (\Delta C)^2} \quad (15)$$

where $i$ and $i+1$ refer to days. $(X_i, Y_i, Z_i)$ and $(X_{i+1}, Y_{i+1}, Z_{i+1})$ are the geocentric satellite positions of the last epoch of day $i$ and the first epoch of day $i+1$, respectively. $M$ is the rotation matrix converted from a geocentric terrestrial reference frame to an orbital frame. The terms $\Delta R$, $\Delta A$, $\Delta C$ and $T_{3D}$ are orbit DBDs in the radial, along- and cross-track as well as three-dimension (3D) directions, respectively.

The mean values of 3D orbit DBDs of satellites C38, C39 and C40 for the solutions with ECOM1, ECOM2 and ECOM1 + BW models inside and outside eclipse seasons are listed in Table 6. For the non-eclipse periods, the ECOM1 + BW solution provides the best orbit quality in the three-dimension direction, followed by the ECOM2 and ECOM1

solutions. Figure 10 shows the DBD ($|\Delta R|, |\Delta A|, |\Delta C|$) statistics of BeiDou-3 IGSOs in the radial, along- and cross-track directions outside eclipse seasons. The ECOM1 + BW model shows the best performance, except that the satellite C39 cross-track orbit consistency for the ECOM1 + BW model is slightly worse than that of the ECOM2 model. The radial and 3D orbit consistency of BeiDou-3 IGSOs for the ECOM1 + BW solution improves by about 2.2 (32.7%) and 5.1 cm (29.5%), 1.2 (21.1%) and 2.6 cm (17.6%) relative to the solutions with the ECOM1 and ECOM2 models on average, respectively.

**Table 6.** Mean 3D orbit DBDs of BeiDou-3 IGSOs for the ECOM1, ECOM2, ECOM1 + BW and ECOM1D + BW solutions in cm. "NE" and "E" denotes the non-eclipse and eclipse seasons, respectively. For C40, values in and out of brackets were for the first two and third eclipse seasons, respectively.

| SRP Model | C38 | | C39 | | C40 | |
|---|---|---|---|---|---|---|
| | NE | E | NE | E | NE | E |
| ECOM1 | 19.1 | 67.3 | 14.9 | 58.8 | 17.8 | 90.0 (20.6) |
| ECOM2 | 16.7 | 66.5 | 12.4 | 57.8 | 15.2 | 90.8 (17.6) |
| ECOM1 + BW | 12.1 | 66.3 | 11.0 | 55.3 | 13.3 | 84.1 (16.7) |
| ECOM1D + BW | - | 17.7 | - | 11.3 | - | 13.3 (13.1) |

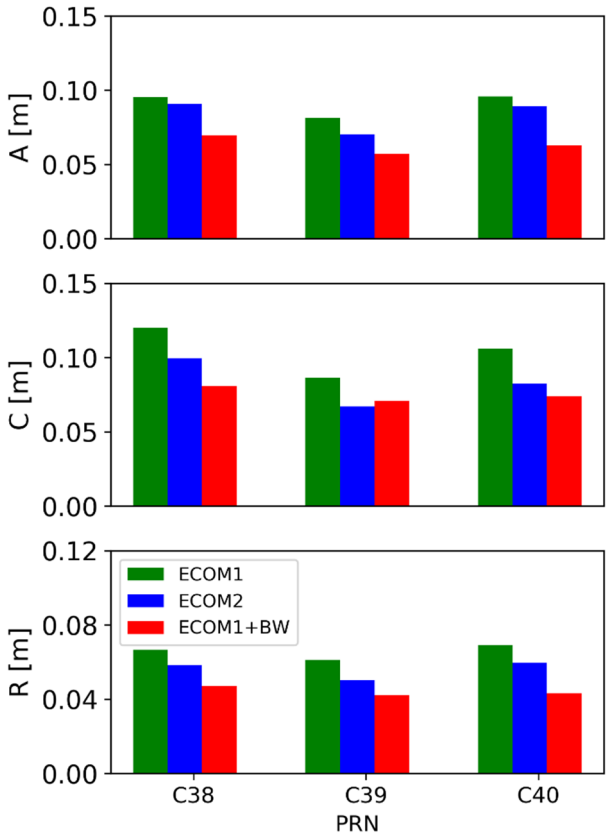


**Figure 10.** Mean orbit DBDs ($|\Delta R|, |\Delta A|, |\Delta C|$) s for the ECOM1, ECOM2 and ECOM1 + BW solutions of BeiDou-3 IGSOs in along-track (A), cross-track (C), and radial (R) directions outside eclipse seasons.

To investigate whether orbit DBDs show $\beta$ -dependent variations like daily clock residuals (Figure 4), the orbit DBD time series of BDS-3 IGSO C39 based on different SRP models in along-track, cross-track, and radial directions are given in Figure 11. It can be clearly seen that there are no $\beta$ -dependent systematic variations in orbit DBDs. This should be due to the fact that the $\beta$ -dependent systematic orbit errors are highly correlated from one day to the next and cannot be reflected in the overlap statistics.

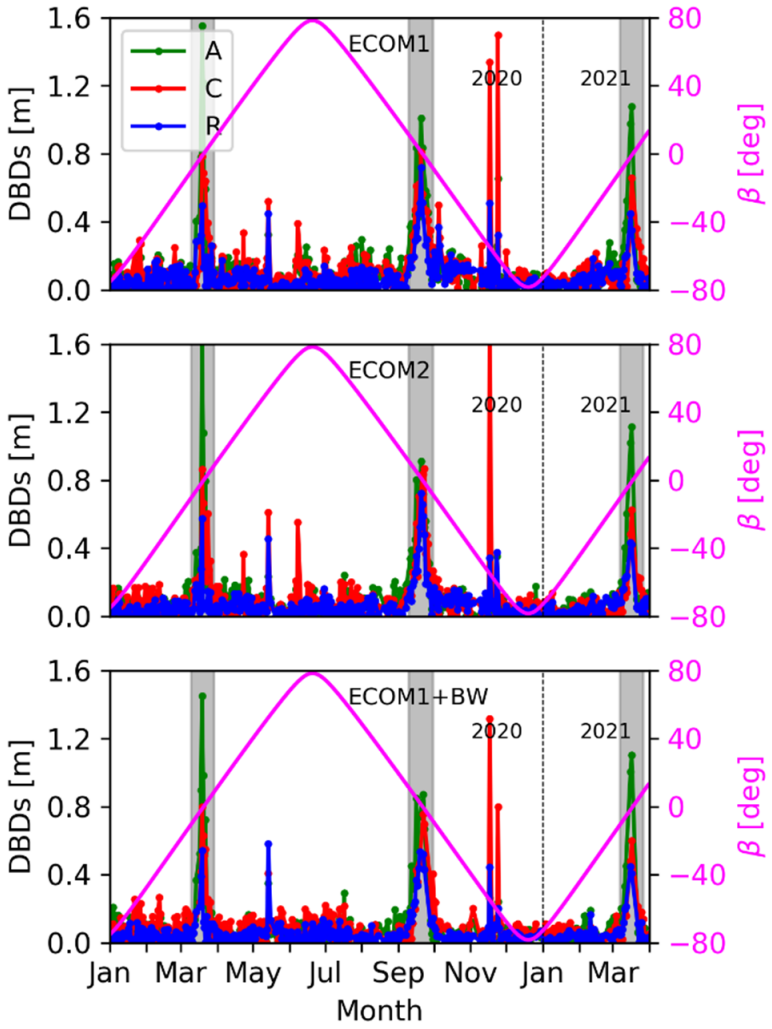


**Figure 11.** Orbit DBD time series ($|\Delta R|, |\Delta A|, |\Delta C|$) s for the ECOM1, ECOM2 and ECOM1 + BW solutions of BeiDou-3 IGSO C39 in along-track (A), cross-track (C) and radial directions.

From Table 6 and Figure 11, the BeiDou-3 IGSO orbit consistency shows a significantly lower performance during eclipse seasons. The orbit 3D DBDs during eclipse seasons are 4–5 times larger than those in the non-eclipse seasons, except that C40 orbit 3D DBDs inside its first (1–23 January 2020) and second (28 June–22 July 2020) eclipse seasons during our experiment only increase by 15–20%. Similar to the clock estimates presented in the previous section, the degraded orbits during eclipse seasons can be improved by using the ECOM1D + BW model. Figure 12 plots the BeiDou-3 IGSO orbit 3D DBDs for the ECOM1 + BW and ECOM1D + BW solutions as a function of $\beta$ -angle. It can be clearly seen that the orbit 3D DBDs of eclipsing C38 and C39, and C40 inside its third eclipse season (27 December 2020–17 January 2021) increase significantly with the decrease of $|\beta|$. Once the ECOM1D + BW model is employed, the elevated orbit errors are basically removed. The mean 3D orbit DBDs of eclipsing C38, C39 and C40 for the ECOM1D + BW solution are given in Table 6. Compared with the ECOM1 + BW solution, the 3D orbit DBDs of satellite C40 inside its third eclipse season, and eclipsing C38 and C39 decreased by 54.7 cm (79.8%) on average, while those of C40 inside its first and second eclipse seasons are reduced by 3.6 cm (21.6%). The orbit consistency inside eclipse seasons can be comparable to that outside eclipse seasons.

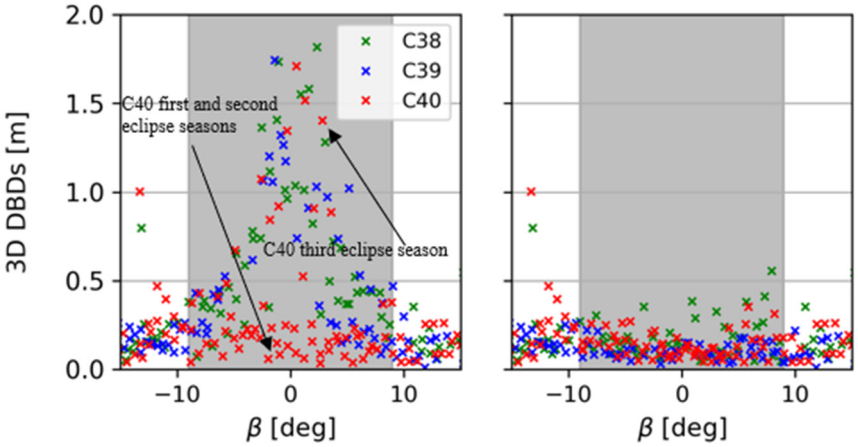


**Figure 12.** Orbit 3D DBDs of BeiDou-3 IGSOs for the ECOM1 + BW (**left**) and ECOM1D + BW (**right**) solutions against $\beta$ -angle. The area shaded in gray indicates eclipse seasons.

## 4. Discussion

Daily clock fitting residual RMS for BeiDou-3 IGSOs based on the ECOM1 model show prominent $\beta$ -dependent effects. This originates from not taking into account the contribution of BeiDou-3 IGSO stretched body, especially at a low $\beta$ -angle, which results in systematic once-per-revolution radial orbit errors. Therefore, a box-wing model is developed for BeiDou-3 IGSOs by estimating the surface optical parameters, which are not yet published or not precisely known. This systematic error is effectively removed overall by augmenting the ECOM1 model with the developed a priori box-wing model. Moreover, the orbit quality improvement during non-eclipse seasons is very significant. Compared to the ECOM1 and ECOM2 solutions, the clock residual RMS decreases by 3.2 cm (47.1%) and 1.4 cm (28.0%), respectively, and the radial and 3D orbit consistency outside eclipse seasons improves by about 2.2 (32.7%) and 5.1 cm (29.5%), 1.2 (21.1%) and 2.6 cm (17.6%), respectively.

However, the orbit performance over the eclipse seasons is much worse than during the non-eclipse periods for the ECOM1, ECOM2 and ECOM1 + BW solutions according to the deteriorated estimates of satellite clocks and elevated orbit DBDs. Attitude analyses show that the yaw behaviors of BeiDou-3 IGSOs have been well reproduced in the study. This rules out the possibility that attitude errors are the reason for the orbit deterioration. Therefore, the orbit degradations are caused by unaccounted non-conservative forces, such as thermal radiation during Earth's shadow transitions.

Considering the signal presented in the BeiDou-3 IGSO clock residuals can be also seen in the Galileo FOC satellites, the method proposed by [22] for servicing eclipsing Galileo FOC satellites, i.e., introducing the $D_s$ term and keeping it active during the Earth's shadow transitions, are used for eclipsing BeiDou-3 IGSO orbit determination. The resulted solution has almost the same performance inside and outside the eclipse reasons measured by the orbit DBDs and the estimated clocks. Therefore, the SRP model which contains the ECOM1 model and $D_s$ term active during eclipse seasons and the developed box-wing model as initial value is recommended for BeiDou-3 IGSO orbit determination.

For BeiDou-3 IGSOs with poor observation geometry, the addition of empirical parameters will potentially increase correlations between the parameters, leading to a weakening of the parameters in the estimation process. Therefore, developing a high-fidelity force model to interpret the unaccounted orbit effects causing the solution deterioration is preferred over the activation of the empirical parameter $D_s$. This requires the BeiDou-3 IGSO manufacturers to disclose the more detailed spacecraft metadata package.

**Author Contributions:** Conceptualization, F.X.; methodology, F.X.; software, M.G. and F.X.; writing—original draft preparation, F.X.; writing—review and editing, M.G. and F.N.; formal analysis, D.C.,

L.T. and C.W.; project administration, S.Y. and F.X. All authors have read and agreed to the published version of the manuscript.

**Funding:** This work of Shirong Ye and Dezhong Chen was funded by the National Key Research and Development Program of China (Grant No. 2019YFC1509603) and the National Science Foundation of China (Grant No. 41974031, 41974038). The work of Chen Wang was supported by Natural Science Basic Research Program of Shaanxi (Grant No. 2022JQ-283). Fengyu Xia is financially supported by the China Scholarship Council (CSC) for his study at the Institute of Geodesy and Geoinformation Science, Technische Universität Berlin.

**Institutional Review Board Statement:** Not applicable.

**Informed Consent Statement:** Not applicable.

**Data Availability Statement:** The raw GNSS data from MGEX stations are publicly available at ftp://cddis.gsfc.nasa.gov (accessed on 15 May 2021). All data from iGMAS stations in this study can be made available with the permission of CSNO.

**Acknowledgments:** We are grateful to the anonymous reviewers for their helpful, constructive suggestions and comments, which significantly improve the paper quality. The numerical calculations in this paper have been done on the supercomputing system in the Supercomputing Center of Wuhan University. Finally, the IGS MGEX and iGMAS are greatly acknowledged for providing the Multi-GNSS data.

**Conflicts of Interest:** The authors declare no conflict of interest.

## References

1. Yang, Y.; Mao, Y.; Sun, B. Basic performance and future developments of BeiDou global navigation satellite system. *Satell. Navig.* **2020**, *1*, 1. [CrossRef]
2. China Satellite Navigation Office. Development of the BeiDou Navigation Satellite System (Version 3.0). Available online: http://www.beidou.gov.cn/xt/gfxz/201812/P020190117356387956569.pdf (accessed on 8 March 2020).
3. Ruan, R.; Jia, X.; Feng, L.; Zhu, J.; Hu, Y.; Li, J.; Wei, Z. Orbit determination and time synchronization for BDS-3 satellites with raw inter-satellite link ranging observations. *Satell. Navig.* **2020**, *1*, 8. [CrossRef]
4. Wang, W.; Wang, Y.; Yu, C.; Xu, F.; Dou, X. Spaceborne atomic clock performance review of BDS-3 MEO satellites. *Measurement* **2021**, *175*, 109075. [CrossRef]
5. Shi, C.; Zhao, Q.; Li, M.; Tang, W.; Hu, Z.; Lou, Y.; Zhang, H.; Niu, X.; Liu, J. Precise orbit determination of Beidou Satellites with precise positioning. *Sci. China-Earth Sci.* **2012**, *55*, 1079–1086. [CrossRef]
6. Shi, C.; Zhao, Q.; Liu, J. Precise relative positioning using real tracking data from COMPASS GEO and IGSO satellites. *GPS Solut.* **2013**, *17*, 103–119. [CrossRef]
7. Fliegel, H.F.; Gallini, T.E.; Swift, E.R. Global positioning system radiation force model for geodetic applications. *J. Geophys. Res. Solid Earth* **1992**, *97*, 559–568. [CrossRef]
8. Beutler, G.; Brockmann, E.; Gurtner, W.; Hugentobler, U.; Mervart, L.; Rothacher, M.; Verdun, A. Extended orbit modeling techniques at the CODE processing center of the International GPS Service for Geodynamics (IGS): Theory and initial results. *Manuscr. Geod.* **1994**, *19*, 367–386.
9. Montenbruck, O.; Steigenberger, P.; Hugentobler, U. Enhanced solar radiation pressure modeling for Galileo satellites. *J. Geod.* **2015**, *89*, 283–297. [CrossRef]
10. Yuan, Y.; Li, X.; Zhu, Y.; Xiong, Y.; Huang, J.; Wu, J.; Li, X.; Zhang, K. Improving QZSS precise orbit determination by considering the solar radiation pressure of the L-band antenna. *GPS Solut.* **2020**, *24*, 50. [CrossRef]
11. Arnold, D.; Meindl, M.; Beutler, G.; Dach, R.; Schaer, S.; Lutz, S.; Prange, L.; So'snica, K.; Mervart, L.; Jäggi, A. CODE's new solar radiation pressure model for GNSS orbit determination. *J. Geod.* **2015**, *89*, 775–791. [CrossRef]
12. Prange, L.; Orliac, E.; Dach, R.; Arnold, D.; Beutler, G.; Schaer, S.; Jäggi, A. CODE's five-system orbit and clock solution—the challenges of multi-GNSS data analysis. *J. Geod.* **2016**, *91*, 345–360. [CrossRef]
13. Wang, C. Solar Radiation Pressure Modelling for BeiDou Navigation Satellites. Ph.D. Dissertation, GNSS Research Center, Wuhan University, Wuhan, China, 2019.
14. Yan, X.; Liu, C.; Huang, G.; Zhang, Q.; Wang, L.; Qin, Z.; Xie, S. A priori solar radiation pressure model for BeiDou-3 MEO satellites. *Remote Sens.* **2019**, *11*, 1605. [CrossRef]
15. Dilssner, F.; Springer, T.; Schönemann, E.; Enderle, W. *Recent Advances in Galileo and BeiDou Precise Orbit Determination at ESA's Navigation Support Office*; EGU: Vienna, Austria, 2020; Available online: https://presentations.copernicus.org/EGU2020/EGU2020-18361_presentation.pdf (accessed on 20 November 2021).
16. Rodriguez-Solano, C.; Hugentobler, U.; Steigenberger, P. Adjustable box-wing model for solar radiation pressure impacting GPS satellites. *Adv. Space Res.* **2012**, *49*, 1113–1128. [CrossRef]

17. China Satellite Navigation Office. BeiDou Satellite Metadata. Available online: http://en.beidou.gov.cn/SYSTEMS/Officialdocument/201912/P020200323536298695483.zip (accessed on 8 March 2021).
18. Wang, C.; Guo, J.; Zhao, Q.; Liu, J. Empirically derivedmodel of solar radiation pressure for BeiDou GEO satellites. *J. Geod.* **2018**, *93*, 791–807. [CrossRef]
19. Duan, B.; Hugentobler, U.; Hofacker, M.; Selmke, I. The adjusted optical properties for Galileo/BeiDou-2/QZS-1 satellites and initial results on BeiDou-3e and QZS-2 satellites. *Adv. Space Res.* **2019**, *63*, 1803–1812. [CrossRef]
20. Rodriguez-Solano, C.J.; Hugentobler, U.; Steigenberger, P.; Allende-Alba, G. Improving the orbits of GPS block IIA satellites during eclipse seasons. *Adv. Space Res.* **2013**, *52*, 1511–1529. [CrossRef]
21. Duan, B.; Hugentobler, U.; Hofacker, M.; Selmke, I. Improving solar radiation pressure modeling for GLONASS satellites. *J. Geod.* **2020**, *94*, 72. [CrossRef]
22. Sidorov, D.; Dach, R.; Prange, L.; Jäggi, A. *Advancing the Orbit Model for Galileo Satellites during the Eclipse Seasons*; EGU General Assembly: Vienna, Austria, 2018; Available online: https://boris.unibe.ch/116170/1/DS_EGU2018.pdf (accessed on 10 November 2020).
23. Sidorov, D.; Dach, R.; Polle, B.; Prange, L.; Jäggi, A. Adopting the empirical CODE orbit model to Galileo satellites. *Adv. Space Res.* **2020**, *66*, 2799–2811. [CrossRef]
24. Dach, R.; Schaer, S.; Arnold, D.; Orliac, E.; Prange, L.; Susˇnik, A.; Villiger, A.; Maier, A.; Mervart, L.; Jäggi, A.; et al. CODE Analysis Center Technical Report. In *International GNSS Service Technical Report*; Jean, Y., Dach, R., Eds.; University of Bern. IGS Central Bureau, Astronomical Institute, 2015; Available online: https://boris.unibe.ch/97576/8/Seiten%20aus%202015_techreport-2.pdf (accessed on 10 November 2020).
25. Marshall, J.; Luthcke, S. Modeling radiation forces acting on TOPEX/Poseidon for precision orbit determination. *J. Spacecr. Rocket.* **1994**, *31*, 99–105. [CrossRef]
26. Milani, A.; Nobili, A.M.; Farinella, P. *Non-Gravitational Perturbations and Satellite Geodesy*; Adam Hilger: Bristol, UK, 1987.
27. Montenbruck, O.; Schmid, R.; Mercier, F.; Steigenberger, P.; Noll, C.; Fatkulin, R.; Kogure, S.; Ganeshan, A.S. GNSS satellite geometry and attitude models. *Adv. Space Res.* **2015**, *56*, 1015–1029. [CrossRef]
28. Jiao, W.; Ding, Q.; Li, J.; Lu, X.; Feng, L.; Ma, J.; Chen, G. Monitoring and Assessment of GNSS Open Services. *J. Navig.* **2011**, *64*, S19–S29. [CrossRef]
29. Montenbruck, O.; Steigenberger, P.; Prange, L.; Deng, Z.; Zhao, Q.; Perosanz, F.; Romero, I.; Noll, C.; Stürze, A.; Weber, G.; et al. The Multi-GNSS Experiment (MGEX) of the International GNSS Service (IGS)—Achievements, prospects and challenges. *Adv. Space Res.* **2017**, *59*, 1671–1697. [CrossRef]
30. Liu, J.-N.; Ge, M.-R. PANDA software and its preliminary result of positioning and orbit determination. *Wuhan Univ. J. Nat. Sci.* **2003**, *8*, 603–609.
31. Petit, G.; Luzum, B. (Eds.) *IERS Conventions*; Verlag des Bundesamts für Kartographie und Geodäsie: Frankfurt, Germany, 2010.
32. Kouba, J. Notes on December 2017 Version of the ECLIPS Subroutine. Available online: http://acc.igs.org/orbits/eclips_Dec_2017.tar (accessed on 10 November 2020).
33. Wang, C.; Guo, J.; Zhao, Q.; Liu, J. Yaw attitude modeling for BeiDou I06 and BeiDou-3 satellites. *GPS Solut.* **2018**, *22*, 117. [CrossRef]
34. Ge, M.; Gendt, G.; Dick, G.; Zhang, F.P. Improving carrier-phase ambiguity resolution in global GPS network solutions. *J. Geod.* **2005**, *79*, 103–110. [CrossRef]
35. Griffiths, J.; Ray, J. On the precision and accuracy of IGS orbits. *J. Geod.* **2009**, *83*, 277–287. [CrossRef]
36. Dilssner, F.; Springer, T.; Gienger, G.; Dow, J. The GLONASS-M satellite yaw-attitude model. *Adv. Space Res.* **2011**, *47*, 160–171. [CrossRef]
37. Prange, L.; Villiger, A.; Sidorov, D.; Schaer, S.; Beutler, G.; Dach, R.; Jäggi, A. Overview of CODE's MGEX solution with the focus on Galileo. *Adv. Space Res.* **2020**, *66*, 2786–2798. [CrossRef]